

Robotic Inside-out Patch Clamp System for Adherent Cells Based on Vesicle Rupture Control

Yuzhu Liu, Ruimin Li, Jinyu Qiu, Biting Ma, Zuqi Wang, Minghui Li, Xin Zhao, and Qili Zhao*

Abstract—The inside-out patch clamp technique has been widely applied in brain science and neuroscience research due to its ability to detect extremely weak currents flowing through a single ion channel. The current manual inside-out patch clamp operations are highly expertise-requisite and low efficient. Meanwhile, the existing robotic systems are only applicable for suspended cells due to their new system setups. For the first time, this paper proposed a robotic inside-out patch clamp system for adherent cells based on vesicle rupture control. Firstly, impedance models were established to detect the vesicle rupture state. Then, a force analysis that combines the defocusing imaging model was developed to precisely control the exposure time of the vesicle in the air, which is a key factor in the rupture process of the vesicle. Based on the above works, a robotic inside-out patch clamp process for adherent cells was established. Experimental results demonstrate that the proposed robotic system can detect vesicle rupture state with a 100% success rate, control exposure time with an average error of 0.02 s and operate adherent HEK-293 cells with a success rate of 70% at an average operation speed of 61.3 seconds/cell. The success rate of our system is more than three times that of manual operation results, laying a solid foundation for subsequent single ion channel functionality research.

Index Terms—Inside-out patch clamp, robotic patch clamp, robotic cell manipulation, micro-operation.

I. INTRODUCTION

THE patch clamp technique, invented by Neher and Sakmann in 1976, has become the “gold standard” in ion channel research in brain science and neuron science due to its ability to detect extremely weak ion channel signals [1]–[3]. The basic research method in ion channel study is the measurement of the current flowing through a single ion channel. To achieve this, the inside-out patch clamp technique is invented. Figure 1 schematically shows the operation process

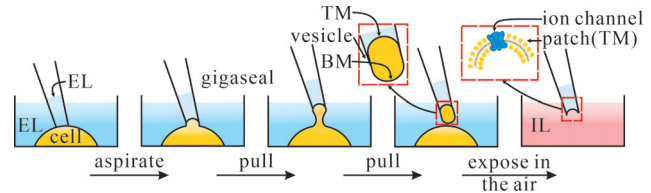


Fig. 1. The schematic of the inside-out patch clamp technique.

of traditional inside-out patch clamp technique [4], [5]. First, the operator uses a micropipette electrode with a micron-sized opening to enter extracellular liquid (EL) and aspirate part of the cell membrane into the micropipette, forming a giga Ω -scale seal (gigaseal) between the cell membrane and inner wall of the micropipette. Then the aspirated cell membrane is pulled off from the cell to form a vesicle by moving the micropipette upward slowly. Then the micropipette tip with vesicle can be moved out of EL and exposed in the air for a certain time to break the bottom membrane (BM) while keeping the top membrane (TM) and the gigaseal, finally forming an inside-out membrane patch. Then the patch is moved into the intracellular liquid (IL) environment to perform an inside-out patch clamp measurement. As the size of the patch is only at a square microns-level, the number of ion channels on it is usually less than ten [6]. Besides, the gigaseal can effectively shield the environmental electrical noises. Therefore, the inside-out patch clamp technique can detect the Picoampere-level current flowing through a single ion channel on the patch, making it widely applied in ion channel study of neuron science research [7]–[9].

At present, a very high level of expertise is required for the manual inside-out patch clamp operation, which usually results in low operation efficiency and significantly limits its wide application. As a result, there is an urgent need for breakthroughs in the automation of the inside-out patch clamp to improve efficiency. However, in comparison to the large number of robotic developed whole-cell patch clamp systems in literatures [10]–[12], only a few robotic inside-out patch clamp systems have been reported according to our best knowledge. For example, Dmitry V. Vasilyev et al. [13] injected suspended cells into a special micropipette electrode, with positive pressure, obtaining a gigaseal from a cell at the inside tip of the electrode. They subsequently ruptured part of the cell membrane outside the micropipette electrode tip, creating an inside-out patch. Besides, the planar patch clamp system can also be used for conducting the inside-out recording mode [14], [15]. The planar patch clamp system allows for the suction of suspended cells to form gigaseal and membrane rupture, enabling the outside of the planar

Manuscript received: August 10, 2024; Revised: November 12, 2024; Accepted: January 09, 2025.

This paper was recommended for publication by Editor X. Liu upon evaluation of the Associate Editor and Reviewers’ comments.

This work was supported by the National Natural Science Foundation of China (62273186), Guangdong Basic and Applied Basic Research Foundation (2024A1515011171), and the Beijing Advanced Innovation Center for Intelligent Robots and Systems (Grant 2019IRS05).

Yuzhu Liu, Ruimin Li, Jinyu Qiu, Biting Ma, Zuqi Wang, Minghui Li, Xin Zhao, and Qili Zhao are with the Institute of Robotics and Automatic Information System (IRASIS), the Tianjin Key Laboratory of Intelligent Robotic (tjKLIR), Nankai University, China, also with the Engineering Research Center of Trusted Behavior Intelligence, Ministry of Education, Nankai University, China, also with the Institute of Intelligence Technology and Robotic Systems, Shenzhen Research Institute of Nankai University, China, and also with the National Key Laboratory of Intelligent Tracking and Forecasting for Infectious Diseases, Nankai University, China. (e-mail: liuyuzhu@mail.nankai.edu.cn; lrumin@163.com; qiujinyu@mail.nankai.edu.cn; 2120230529@mail.nankai.edu.cn; 2120210425@mail.nankai.edu.cn; lmh1391407002@163.com; zhaoxin@nankai.edu.cn; *Contacting Author: zhaoqili@nankai.edu.cn)

Digital Object Identifier (DOI): see top of this page.

surface exposure to the intracellular environment. Unfortunately, both of the aforementioned methods are limited to suspended cells. In summary, existing robotic inside-out patch-clamp systems are not applicable to adherent cells or cells *in vivo* due to their new system setups, which are crucial for maintaining electrophysiological connections. Adherent cells are particularly significant in brain science and neuroscience, as they better reflect physiological behaviors and enhance our understanding of intercellular interactions and their changes in disease models. Thus, utilizing adherent cells in the study increases its application value. As a result, a robotic inside-out patch clamp operation method that is applicable to adherent cells is still highly desired.

According to the operation of the inside-out mode, vesicle rupture is essential for forming an inside-out patch and is a primary factor determining the success rate of the operation. Successful vesicle rupture directly indicates the formation of the desired inside-out patch. To improve the success rate of the inside-out patch clamp operation, the vesicle rupture process should be precisely controlled. To achieve this, the rupture state of the vesicle should be detected first. However, as the micropipette electrode is usually installed at a tilt angle, the focus extent of the micropipette tip is not consistent. Thus, it is difficult to observe and detect whether the vesicle has ruptured through microscopic view feedback. Therefore, a new vision-free detection method is required to estimate the rupture state of the vesicle. Besides, the exposure time of the vesicle in the air can affect the rupture state of the vesicle significantly [5]. As shown in Fig. 1, the whole vesicle membrane can be divided into two parts, the TM aspirated into the micropipette opening and the BM which is the rest of the vesicle membrane outside of the micropipette opening. A too short exposure time may not rupture the BM of the vesicle to form the inside-out patch, while a too-long one may cause both TM and BM to rupture, resulting in patch collapse and subsequent electrophysiological recording failure. To determine an appropriate exposure time for vesicle rupture, the duration of the exposure, from the micropipette tip leaving the liquid to entering the liquid, should be precisely controlled. To accomplish this, the moments of the micropipette tip leaving and entering the liquid should be detected through image processing methods. However, related research work is still missing according to references.

Our group has conducted extensive research on robotic patch-clamp techniques over an extended period. In previous studies, we successfully developed robotic whole-cell and cell-attached configurations for both adherent cells and neurons in mouse brain slices [16], [17]. Building on this foundation, we recently initiated research on single-channel patch-clamp techniques, introducing a robotic inside-out patch clamp system based on vesicle rupture control. Firstly, impedance models were established to estimate the vesicle rupture state based on transmembrane current responses. Then, a force analysis combined defocusing imaging model of the liquid adhering to the micropipette tip while leaving and entering the liquid was developed to precisely control the exposure time of the vesicle in the air. Using these techniques, an appropriate exposure time of the vesicle in the air was determined to form the inside-

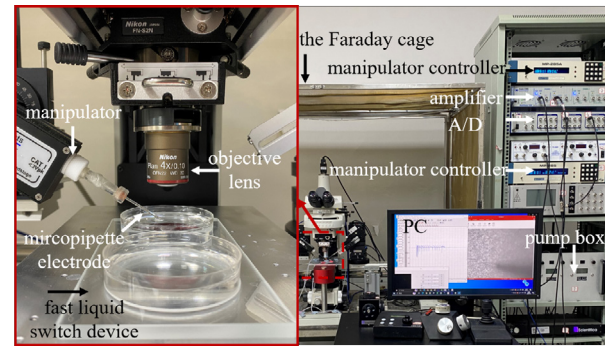


Fig. 2. Robotic inside-out patch clamp system.

out patch. Based on the above works, a robotic inside-out patch clamp system for adherent cells was established based on rupture control of vesicles. Experimental results demonstrate that the proposed robotic inside-out patch clamp system is able to detect vesicle rupture state with a 100% success rate, control exposure time with an average error of 0.02 s, operate adherent HEK-293 cells with a success rate of 70%, and at an average operation speed of 61.3 seconds/cell. The success rate of our system is three times that of manual operation results, laying a solid foundation for subsequent single ion channel functionality research.

II. SYSTEM SETUP

The robotic inside-out patch clamp system is developed within our laboratory [18], as shown in Fig. 2. A standard upright microscope (Eclipse FN1, Nikon) capable of moving in an area of 20 mm × 20 mm in the X-Y plane with repeatability of $\pm 1 \mu\text{m}$ is utilized to observe the cell in the patch clamp operation. An X-Y-Z micromanipulator (MP285, Sutter Instrument, Sacramento, CA, USA) with a travel space of 50 mm × 50 mm × 50 mm and a repeatability of $\pm 1 \mu\text{m}$ is used to install the micropipette electrode. A motorized focusing device with the repeatability of $\pm 1 \mu\text{m}$ (ES10ZE, Prior, Cambridge, UK) is utilized in controlling the movement of the objective lens in the Z axis to focus on the cell in the vertical direction. A self-designed pump box [16] provides pressure inside the micropipette electrode for patch clamp operation. A charge-coupled device (CCD) camera (IR-2000, DAGE-MTI) is mounted on the microscope and captures microscopic images at a rate of 60 frames per second, providing visual feedback for the patch clamp operation. A host computer is used for microscopic image processing, electrical signal acquisition, aspiration pressure control, and motion control of the microscope and the manipulator. The whole robotic system is covered by a Faraday cage to isolate electric disturbances from the outside environment.

The micropipette used in the patch clamp operation is prepared from a borosilicate glass tube (Sutter, BF150-86-10), with an outer diameter of 1.5 mm and an inner diameter of 0.86 mm. This glass tube is pulled by a micropuller (Sutter, P97) to form a micropipette with a resistance of 3–8 M Ω . The micropipette is first back-filled with 20 μL of extracellular liquid (EL) [19]. After filling with EL, a silver electrode wire with an outer diameter of 0.2 mm is plugged into the

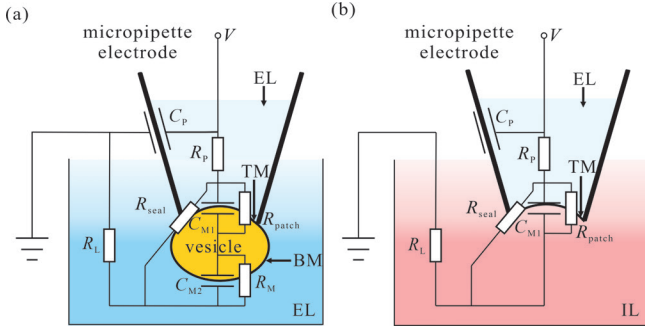


Fig. 3. The schematic of impedance model. (a) Before vesicle rupture. (b) After vesicle rupture.

micropipette to form a micropipette electrode which is then mounted on the manipulator with a tilt angle of 45° . The EL should be allowed to contact the silver electrode and complete the electrical circuit, thus forming the micropipette electrode. Before manipulation, the liquid in the petri dish with cells is changed to EL. The intracellular liquid (IL) [19] is added to an empty petri dish for electrical signal recording. The electrical signals detected by the micropipette electrode are amplified by an amplifier (MultiClamp 700B, Molecular Devices), then converted into digital signals, and finally transmitted to the host computer.

Before the vesicle is exposed to the air, the outer side of the cell membrane should be in contact with EL. After the vesicle is exposed to the air and ruptures, the inner side of the cell membrane facing outside should be in contact with IL. To keep the normal function of the cell membrane, the liquid environment surrounding the micropipette tip should switch from EL to IL during the above vesicle rupture process. To achieve this task, a simple fast liquid switching device is designed, as shown in Fig. 2. The device is equipped with two grooves for holding petri dishes with a diameter of 60 mm. One groove holds one petri dish containing EL and cells, and the other groove holds another petri dish with IL. By moving this device, the liquid environment can be rapidly switched during the micropipette electrode moving up with the vesicle exposed in the air.

III. METHODOLOGIES AND KEY TECHNOLOGIES

A. Microscopic vision-free rupture detection of vesicle based on impedance model

As mentioned before, vesicle rupture is a crucial step in the formation process of an inside-out patch. However, it is challenging to directly observe the rupture state of the vesicle under a microscope as mentioned in the Introduction. Therefore, an impedance model before and after the vesicle rupture was established [20] to estimate the rupture state of the vesicle without view feedback.

Before the vesicle rupture, the total measured impedance Z_1 can be calculated according to

$$Z_1 = \frac{1}{j\omega C_P} \parallel \left\{ R_P + R_L + \left\{ R_{\text{seal}} \parallel \left[(R_{\text{patch}} \parallel \frac{1}{j\omega C_{M1}}) + (R_M \parallel \frac{1}{j\omega C_{M2}}) \right] \right\} \right\} \quad (1)$$

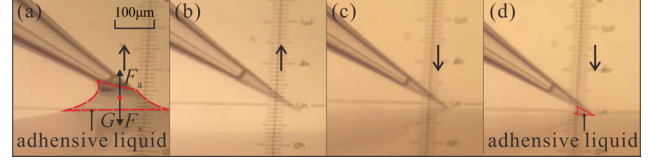


Fig. 4. The tip of the micropipette leaving and entering the liquid (side view). (a) Before leaving. (b) After leaving. (c) Before entering. (d) After entering.

as shown in Fig. 3(a), the symbols + and \parallel represent series and parallel connections, respectively; R_P represents the internal resistance of the micropipette, encompassing the resistance of the silver wire and the liquid resistance inside the micropipette; C_P represents the capacitance of the micropipette wall; R_L represents the total resistance in the external liquid environment surrounding the micropipette; R_{seal} represents the seal resistance resulting from the gigaseal; R_{patch} and C_{M1} represent the resistance and capacitance of the TM, respectively, while R_M and C_{M2} represent those of the BM. Based on experimental results, the cytoplasmic resistance of the vesicle can be neglected compared to the gigaseal and vesicle membrane resistance.

After the rupture, as shown in Fig. 3(b), the total measured impedance Z_2 can be calculated according to

$$Z_2 = \frac{1}{j\omega C_P} \parallel \left\{ R_P + R_L + [R_{\text{seal}} \parallel (R_{\text{patch}} \parallel \frac{1}{j\omega C_{M1}})] \right\} \quad (2)$$

Under constant voltage, capacitance can be treated as open circuits, and only the resistance is considered for analysis. Therefore, the total resistance before vesicle rupture R_1 can be calculated according to

$$R_1 = R_P + R_L + [R_{\text{seal}} \parallel (R_{\text{patch}} + R_M)] \quad (3)$$

The total resistance after vesicle rupture R_2 can be calculated according to

$$R_2 = R_P + R_L + (R_{\text{seal}} \parallel R_{\text{patch}}) \quad (4)$$

It can be observed from Eq. (3) and Eq. (4) that the values of R_1 and R_2 are very close because the value of R_M is much smaller compared to R_{patch} and R_{seal} [20]. Thus, the measured resistance under constant voltage can not be utilized to estimate the rupture state of the vesicle. The capacitance can be analyzed in impedance models under the step voltage input [21]. The capacitances in the models consists of micropipette electrode capacitance C_P , TM capacitance C_{M1} and BM capacitance C_{M2} . The former is compensated by the patch clamp amplifier MultiClamp700B which can be ignored in the following analysis. Before vesicle rupture (see Fig. 3(a)), the effect of membrane capacitance can be ignored. This is because R_{patch} , C_{M1} and R_M , C_{M2} form two RC parallel circuits in series, with nearly equal values of the products of resistance and capacitance [21]. In that case, the capacitance effect of the above two RC circuits can basically compensate for each other under the step voltage input. After the vesicle rupture (BM breaks and TM stays)(see Fig. 3(b)), it is equivalent to only one RC circuit.

According to the zero-state response of an RC circuit, when a step voltage of amplitude U is applied, the resulting transmembrane current response, denoted as $I_{RC}(t)$ and representing the flow of electrical current across the cell membrane in response to the voltage change, can be expressed as follows:

$$I_{RC}(t) = -\frac{U}{R_{\text{patch}}} e^{-\frac{t}{R_{\text{patch}}C_{M1}}} \quad (5)$$

In summary, before the vesicle rupture, the transmembrane current under the step voltage input will be closed to zero because of the capacitance compensation. After vesicle rupture, the transmembrane current will exhibit a zero-state response curve described by Eq. (5). Therefore, the response of the transmembrane current under the step voltage input is used to estimate the rupture state.

B. Vesicle exposure time control based on force analysis combined with defocusing imaging model

In this paper, the air exposure method is employed to induce vesicle rupture. This involves moving the vesicle from EL to the air, exposing it for a certain interval, and then moving it back into IL. The rupture state is directly related to the exposure time according to literature [5]. Insufficient exposure time can result in no rupture of BM, while excessive exposure time can lead to the further rupture of TM after BM ruptures, both leading to inside-out mode failure. Therefore, it is crucial to accurately control the exposure time of vesicles in the air to find the optimal vesicle exposure time for improving the success rate of inside-out recording mode.

1) Force analysis for liquid adhering to micropipette tip :

The exposure time of the vesicle in the air is defined as the time interval from the micropipette tip with the vesicle leaving EL to it entering IL. The outer surface of a micropipette made from a glass tube is usually hydrophilic. When the micropipette tip is in proximity to the liquid, an adhesive force is generated.

When the micropipette leaves EL, even after it has moved above the plane where the previous liquid surface was, a small amount of liquid still adheres to the micropipette tip due to the adhesive force between them, as shown in Fig. 4(a), (b).

Similarly, during the micropipette entering IL, the micropipette tip attracts part of the liquid to adhere to it before it reaches the former liquid surface, as shown in Fig. 4(c), (d). It is worth noting that Fig. 4 is videotaped from a special side-view microscope, which is usually not available for patch clamp systems. We show it here just for the purpose of supporting our previous analysis.

The amount of adhesive liquid between the tip and the previous liquid plane increases as the micropipette tip arises because of the adhesive force as shown in Fig. 4(a). When the gravity (G) and surface tension (F_s) of the above retained liquid become larger than the adhesive force (F_a), the retained liquid detaches and falls from the micropipette tip. Therefore, the moment that the micropipette tip leaves the liquid is actually the moment when the force balance is disrupted and the liquid droplet detaches. Similarly, the moment of entering

liquid is when the liquid is attracted and adhered to the micropipette tip.

2) *The leaving and entering moment detection based on defocusing imaging model:* To keep the micropipette tip with adhesive liquid in the field of view, the micropipette tip moves up along Z axis direction to leave the EL. To facilitate the observation of $1\ \mu\text{m}$ -sized micropipette tip, the inside-out patch clamp is usually performed under a high-power objective lens, which is usually $40\times$ objective lens. However, a high-power objective lens usually has a short moving distance in Z axis direction due to its large size in height and that EL, as well as IL, are usually stored in petri dishes with high side walls. Therefore, when the micropipette tip moves up to a position above the petri dish side wall during the liquid switch, it is usually in a defocused state because the objective lens can not follow the micropipette tip in a vertical direction due to its aforementioned short working distance in Z direction. Thereby, the aforementioned detaching and attraction moment need to be determined when the micropipette tip is in the defocused state, making the common image processing methods relying on the focused state of the target not feasible.

When an object is out of focus, its contrast to its background in the microscopic image can be estimated according to [9]

$$C(x, y) = \frac{I(x, y) - I_0(x, y)}{I_0(x, y)} = \Delta f \Delta n \nabla^2 h(x, y) \quad (6)$$

where C is the contrast between the target and the background, I is the gray value, Δf is the defocusing distance, Δn is the difference of refractive index between the object and its surrounding background, and $\nabla^2 h(x, y)$ is the curvature of the object's surface. The contrast of the image at point (x, y) , denoted as $C(x, y)$, is given by the equation mentioned above. Here, $I_0(x, y)$ represents the gray scale value of the current frame at point (x, y) , and $I(x, y)$ represents the gray scale value of the same point in the next frame. If the frame rate is high enough, the defocusing distance Δf and the refractive index difference between the micropipette with adhesive liquid and the surrounding background Δn can be neglected in neighboring frames. Only the curvature of the micropipette with adhesive liquid $\nabla^2 h(x, y)$ will undergo sudden changes when the micropipette leaves or enters the liquid. Therefore, the variation in the average contrast of the images is used to determine the moments of the micropipette leaving and entering the liquid. The above leaving and entering moments are confirmed when the variation values become larger than the set threshold values.

3) *Vesicle exposure time control method:* As shown in Fig. 5, the exposure time of the vesicle in the air is the time cost in the micropipette leaving EL at the point P_L , moving up to the top point P_T , stopping at P_T and staying for a certain time, and finally moving downward to enter IL at the point P_E . To facilitate the motion control of the micropipette while it leaves EL and enters IL, it is controlled to first accelerate with a constant acceleration a_C , then move with a constant speed v_C , and decelerate with the same deceleration a_C to stop. To accelerate the whole process, the a_C is set as the maximum acceleration of the manipulator, ensuring that the acceleration stage of the micropipette is short enough to guarantee its entry

into the constant speed stage when passing P_L and P_E . The exposure time t_E is calculated based on the above assumption.

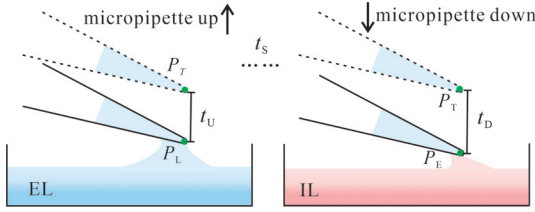


Fig. 5. Schematic of motion trajectory of micropipette during vesicle rupture process

According to Fig. 5, the exposure time consists of three parts as

$$t_E = t_U + t_S + t_D \quad (7)$$

where t_U is the time cost from point P_L to the top point P_T , t_S is the stay time at the top point P_T , and t_D is the time cost from point P_T to the entry point P_E . The time t_U consists of two parts as

$$t_U = t_{U_C} + t_{U_D} \quad (8)$$

where t_{U_D} is the deceleration time which can be obtained according to

$$t_{U_D} = \frac{v_C}{a_C} \quad (9)$$

The time, t_{U_C} , representing the duration of its motion at the constant speed v_C , can be calculated as

$$t_{U_C} = \frac{h_{P_T} - h_{P_L} - \frac{v_C^2}{2a_C}}{v_C} \quad (10)$$

where h_{P_T} and h_{P_L} are heights of P_T and P_L , respectively.

Substituting Eq. (9) and Eq. (10) into Eq. (8), t_U can be obtained as

$$t_U = \frac{v_C}{a_C} + \frac{h_{P_T} - h_{P_L} - \frac{v_C^2}{2a_C}}{v_C} \quad (11)$$

Similarly, t_D can be calculated according to

$$t_D = \frac{v_C}{a_C} + \frac{h_{P_T} - h_{P_E} - \frac{v_C^2}{2a_C}}{v_C} \quad (12)$$

Substituting Eq. (11) and Eq. (12) into Eq. (7), the exposure time can be obtained as

$$t_E = t_S + 2\frac{v_C}{a_C} + \frac{2h_{P_T} - h_{P_L} - h_{P_E} - \frac{v_C^2}{a_C}}{v_C} \quad (13)$$

In comparison to the whole volume of EL and IL in petri dishes, the liquid loss of EL and IL caused by evaporation and micropipette leaving and entering the liquid during the whole patch clamp operation can be ignored. Thus, for the same micropipette, the heights of P_L and P_E can be treated as constants for the same two petri dishes of EL and IL. After calibration of their heights before experiments through the aforementioned defocusing imaging methods, the exposure time t_E can be quantitatively controlled by setting values of h_{P_T} and t_S according to Eq. (13). Finally, the whole

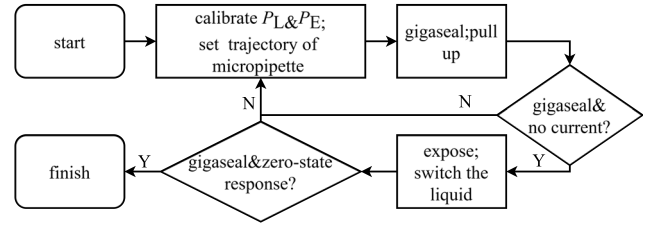


Fig. 6. The robotic inside-out patch clamp operation procedure.

motion trajectory of the micropipette during vesicle rupture is designed by setting values of h_{P_T} and t_S .

C. Robotic inside-out mode based on vesicle rupture control

Based on the above works, the robotic inside-out patch clamp operation procedure is established, as shown in Fig. 6.

Before cell operation, P_L and P_E are calibrated by detecting the moment of leaving from EL and the moment of entering IL using the methods described in Section III(B). Given an exposure time t_E , constant speed v_C , and top point P_T , the system automatically calculates the stop time t_S and further designs the whole motion trajectory of the micropipette. Then the micropipette moves back to EL again to start the robotic inside-out patch clamp operation.

At first, the system automatically focuses and localizes the adherent cells using the previously-developed defocusing localization method [22]. Further, the micropipette electrode automatically approaches and makes contact with the surface of the target cell, aspirating a part of the cell membrane to form a gigaseal. The detailed process of the gigaseal formation has been described in our previous publication above [18]. Here, we will not delve into it again.

After the gigaseal has formed, the micropipette electrode is moved upward at the maximum motion speed of $3000 \mu\text{m/s}$ to pull the aspirated cell membrane out of the cell to form a vesicle. Before leaving EL, the micropipette electrode applies a constant voltage. If the micropipette electrode tip forms a vesicle, it should appear as a gigaseal state, as mentioned in Section III(A). In this case, the transmembrane current should be represented close to zero when the step voltage is applied to the micropipette electrode. The formation of vesicle is judged by the above two reactions. If the micropipette electrode tip fails to form a vesicle, it should appear as losing the gigaseal. Then the system will automatically choose another cell to repeat the above process.

Next, the micropipette electrode moves upward to exit EL environment following the set trajectory. After it has arrived at the set top point P_T with the safe height which is higher than the side wall of the petri dish, the liquid below the micropipette electrode is switched from EL to IL through the aforementioned switching device. After the pause interval, the micropipette electrode moves downward. In this way, the tip of the micropipette electrode enters IL environment and the resistance value can be observed. If the inside-out patch is formed at the micropipette opening, the resistance value remains in the gigaseal state. In that case, when the step

voltage is applied, the current signal will be represented as a zero-state response curve given in Eq. (5).

If the vesicle does not rupture (BM does not break) without any capacitance charging or discharging phenomenon and maintains gigaseal, it is necessary to increase the vesicle exposure time in the air next time for another vesicle of stripped from another cell. On the other hand, if the vesicle ruptures completely (TM breaks), resulting in the disappearance of the gigaseal, it is necessary to decrease the vesicle's exposure time in the air for the next attempt.

IV. EXPERIMENTAL RESULTS

In this section, a series of experiments on HEK-293 cells were conducted to validate the effectiveness of the proposed robotic inside-out patch clamp system and the above methodologies and key technologies in Section III. First, the rupture state detection experiments were finished to validate the effectiveness of the microscopic vision-free rupture detection of vesicles based on the impedance model. Then, the exposure time control experiments were performed to evaluate the control error and the repeatability of the exposure time control method in Section III(B). Finally, robotic inside-out patch clamp experiments were conducted and compared with manual operation results to validate the effectiveness of the proposed robotic system.

The HEK-293 cells utilized in the following experiments were provided by the cell bank of the Chinese Academy of Sciences and prepared according to the protocol given in literature [23]. The following experiments were conducted at a room temperature of 26 °C, with both EL and IL heated to 37 °C.

A. Vesicle rupture detection results

A number of 15 HEK-293 cells cultured in 3 petri dishes and confirmed with effect vesicles after membrane stripping were randomly selected (5 cells in each petri dish) as the target cells for the vesicle rupture detection experiments. The 15 cells were evenly distributed into three groups (5 cells in each group). For the first group of 5 cells, their vesicles were tested three times without any exposure to the air. For the second group of 5 cells, their vesicles were first exposed to the air for about 4 seconds, which has been experimentally determined to be able to only rupture TM of vesicles to form inside-out patches (see more details in Section IV(B)), and then tested for three times using proposed rupture state detection method. For the third group of cells, their vesicles were first deliberately over-exposed for a long time (which is experimentally determined to be 10 seconds according to the testing results in Section IV(B)) to break both BM and TM of vesicles, making the patch failure, and then tested for three times using the proposed rupture state detection method.

Figure 7 shows the response curves of the transmembrane current under a step voltage when the vesicle is integrated (group 1), only BM ruptures (group 2), and both BM and TM rupture (patch fails in group 3), respectively. The total number of 45 testing results are all correct, proving a 100% success rate of the proposed vesicle rupture detection. For each

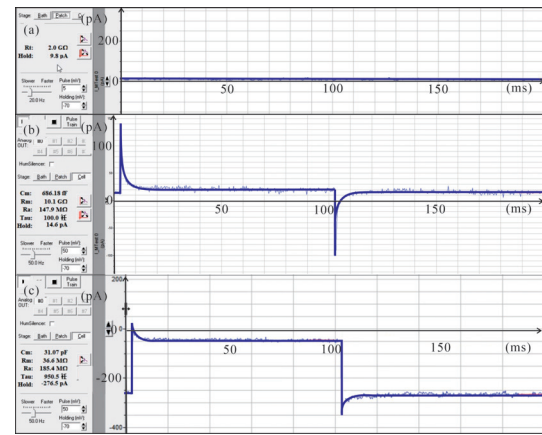


Fig. 7. The zero-state response curves of the transmembrane current. (a) Vesicle formation. (b) Inside-out patch. (c) Patch failure.

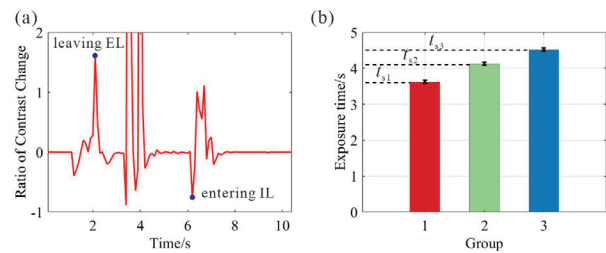


Fig. 8. Exposure time control results. (a) The contrast variation of micropipette during vesicle rupture process. (b) Exposure time control results.

cell, all three testing results are consistent, proving a good repeatability of the proposed detection method. The reader can find more details about the above measurement process in the supplementary file “rupture state detection for vesicle.avi”.

B. Vesicle exposure time control experiments

To evaluate the control error of exposure time, the detected actual exposure time of three micropipettes was compared with the setting exposure time. The threshold values to judge the leaving moment from EL and entering moment into IL were set as 1.5 and 0.5, respectively. The three micropipettes were tested in three pairs of petri dishes containing EL and IL. Three different exposure time, 3.6 s, 4.1 s and 4.5 s were set in experiments. The tests were repeated five times for each set and micropipette to test the repeatability of the proposed method. The detected contrast ratio variation for one micropipette is shown in Fig. 8(a).

The reader can find more details of the exposure time control method in the supplementary file “exposure time control.avi”. The detected actual exposure time for one micropipette with different sets of exposure time is shown in Fig. 8(b). It can be found that the actual average exposure time follows the set values well with the average error of 0.02 s. Further, the standard error of every five repeated experiments is less than 0.045 s (less than 2.9% of the set values) for all micropipettes, which proves our method has good repeatability.

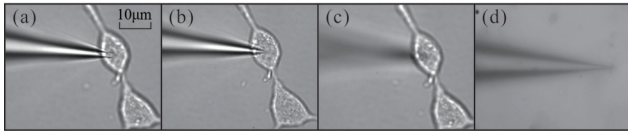


Fig. 9. The experimental images of robotic inside-out patch clamp operation. (a) Cell contact. (b) Gigaseal formation. (c) Vesicle formation. (d) Vesicle rupture.

C. Robotic inside-out patch clamp experiments

A total number of 10 HEK-293 cells cultured in three petri dishes were randomly selected for robotic inside-out patch clamp operation. As a comparison, a total number of 10 cells were operated manually by an operator with more than one year experience. The detailed robotic operation procedure has been given in Section III(C). Figure 9 shows the experimental images of the detailed operation process. In experiments, the exposure time was set as 4 s, which is experimentally determined as an appropriate value for vesicle rupture according to a large number of tests. The exposure time of the manual operation is determined according to experience. A successful inside-out patch clamp operation is confirmed if an inside-out patch is found after the vesicle rupture control. Otherwise, the operation is considered as a failure.

The experimental results demonstrate that our robotic system is capable of operating HEK-293 cells with a success rate of 7/10, at an average speed of 61.3 s/cell. The three failure cases are due to low-quality gigaseals, which compromised vesicle formation during the pulling process. In comparison, the manual operation achieved a success rate of only 2/10 at an average speed of 62.5 s/cell. Success rates reported for inside-out mode [13] typically range from 70% to 80%. While our success rate is comparable to other robotic systems, our approach is specifically designed for adherent cells, making it more meaningful for research in brain science and neuroscience.

In comparison to the manual method, the higher accuracy and repeatability of the exposure time control, as well as the high quality of gigaseal, of our robotic method may be attributed to the advantage in success rate. Although with an extra calibration of P_L and P_E , which usually takes about 10 seconds on average, our robotic operation method has comparable speed as the manual operation method due to higher speeds in other parts of procedures, such as the gigaseal formation process.

V. DISCUSSIONS

This paper proposed a robotic inside-out patch clamp system based on vesicle rupture control. Different from the other current automated inside-out systems relying on new special devices [13]–[15], which makes them only applicable for suspended cells, our system uses the traditional operational procedure of inside-out mode. This advantage highlights the strong adaptability of our system, making it highly suitable not only for adherent cells but also for a diverse array of other cell types. For adherent cells with different membrane characteristics, it is necessary to adjust the dimensions of the micropipette electrodes and the related liquid formulations to

ensure a successful gigaseal and exposure time of the vesicle in the air to guarantee vesicle rupture. For the suspended cells, by adding a holding micropipette to immobilize them, our system may also be utilized to operate them in the future. After combining an IL storage device with the current holding device for brain slices, our system can even be applied to operate neurons in brain slices, which has more important research value in brain science compared to adherent cells. With further development, particularly through integration with two-photon microscopy and the design of compatible intracellular liquid storage devices, this system could potentially be adapted for *in vivo* applications. Moreover, by incorporating a device for cleaning the micropipettes, the pre-calibrated micropipettes can be reused and the calibration process of P_L and P_E can be omitted, leading to a substantial reduction in the operational time for one cell.

In this paper, we use the microscopic image to control the exposure time by detecting the leaving moment from EL and the entering moment to IL. As a matter of fact, when the micropipette electrode tip leaves EL, an open circuit is formed, and when it enters IL, the circuit is restored, generating an electrical current. Therefore, the time from the formation of the open circuit to its restoration can be used to estimate the exposure time. The electric current variation may be utilized to detect the leaving moment and entering moment for exposure time control. Unfortunately, the commonly used proprietary software for measuring the electric signals of patch clamps often makes it difficult to obtain accurate moments for circuit interruption and restoration. Therefore, the control accuracy of exposure time using these methods depends on the significant time intervals provided by the proprietary software, which can easily generate large control errors in exposure time, subsequently reducing the formation success rate of the inside-out patch. In comparison, the control error of exposure time using the microscopic image processing method mainly results from the image capture interval, which is only 1/60 second in this paper. Based on the above consideration, we chose the microscopic image processing method to control the exposure time of the vesicle.

The inside-out patch clamp operation success rate of our system can be further improved in the following aspects. First, the primary cause of inside-out patch clamp failures in our system is the formation of low-quality gigaseals. Since a portion of the cell membrane must be pulled away to create a vesicle, the inside-out mode requires a more stable gigaseal compared to whole-cell and cell-attached modes. Enhancing gigaseal quality could involve optimizing liquid composition, applying electrical stimulation, using visual methods to select high-quality cells, and adjusting the direction and speed of the micropipette's movement. These methods can enhance the quality of the gigaseal or reduce damage to it, potentially increasing the success rate of our system in future applications. Besides, the current exposure time of the vesicle in the inside-out patch clamp operation is set as a constant which is roughly determined through experiments, which may miss the optimal value due to the limited number of experiments. Through doing more tests in the future, a set value more close to the optimal value can be determined to further improve the success

rate of our robotic system.

VI. CONCLUSIONS

For the first time, this paper proposed a robotic inside-out patch clamp system for adherent cells based on vesicle rupture control. Impedance models were established to detect the vesicle rupture state with a 100% success rate. With a developed force analysis combined with a defocusing imaging model of the liquid adhering to the micropipette tip, the control error of exposure time of the vesicle in the air, which has a significant influence on the rupture state of the vesicle, is reduced to 0.02 s on average. Based on the above works, a robotic inside-out patch clamp process for adherent cells was established based on rupture control of the vesicle. Experimental results demonstrate that the proposed robotic inside-out patch clamp system is able to operate adherent HEK-293 cells with a success rate of 70%, having significant advantages compared to manual operation results. The above advantages of our system lay a solid foundation for subsequent single ion channel functionality research in the future.

REFERENCES

- [1] E. Neher and B. Sakmann, "Single-channel currents recorded from membrane of denervated frog muscle fibres," *Nature*, vol. 260, no. 5554, pp. 799–802, 1976.
- [2] E. Neher and B. Sakmann, "The patch clamp technique," *Scientific American*, vol. 266, no. 3, pp. 44–51, 1992.
- [3] G. J. Stuart and B. Sakmann, "Active propagation of somatic action potentials into neocortical pyramidal cell dendrites," *Nature*, vol. 367, no. 6458, pp. 69–72, 1994.
- [4] F. J. Sigworth and E. Neher, "Single na⁺ channel currents observed in cultured rat muscle cells," *Nature*, vol. 287, no. 5781, pp. 447–449, 1980.
- [5] Z. Liu, *Practical Patch Clamp Techniques*. Beijing Science and Technology Press, 2016.
- [6] R. I. Slavchov, T. Nomura, B. Martinac, M. Sokabe, and F. Sachs, "Gigaseal mechanics: creep of the gigaseal under the action of pressure, adhesion, and voltage," *The Journal of Physical Chemistry B*, vol. 118, no. 44, pp. 12 660–12 672, 2014.
- [7] C. G. Parsons, K. E. Gilling, and C. Jatzke, "Blocking kinetics of memantine on nr1a/2a receptors recorded in inside-out and outside-out patches from xenopus oocytes," *Journal of Neural Transmission*, vol. 115, pp. 1367–1373, 2008.
- [8] A. Kokhan, S. Zdanevich, I. Prokofev, I. Gorudko, and E. Shamova, "Patch-clamp technique for studying ion channels in activated platelets," *Syst. Biol. Physiol. Rep.*, vol. 1, no. 1, pp. 3–11, 2021.
- [9] C. B. Schroeter, C. Nelke, M. Schewe, L. Spohler, A. M. Herrmann, T. Müntefering, N. Huntemann, M. Kuzikov, P. Gribbon, S. Albrecht *et al.*, "Validation of trek1 ion channel activators as an immunomodulatory and neuroprotective strategy in neuroinflammation," *Biological Chemistry*, vol. 404, no. 4, pp. 355–375, 2023.
- [10] H.-J. Suk, E. S. Boyden, and I. van Welie, "Advances in the automation of whole-cell patch clamp technology," *Journal of neuroscience methods*, vol. 326, p. 108357, 2019.
- [11] L. A. Annecchino, A. R. Morris, C. S. Copeland, O. E. Agabi, P. Chaderton, and S. R. Schultz, "Robotic automation of in vivo two-photon targeted whole-cell patch-clamp electrophysiology," *Neuron*, vol. 95, no. 5, pp. 1048–1055, 2017.
- [12] R. Yang, K. W. Lai, N. Xi, and J. Yang, "Development of automated patch clamp system for electrophysiology," in *2013 IEEE International Conference on Robotics and Biomimetics (ROBIO)*. IEEE, 2013, pp. 2185–2190.
- [13] D. V. Vasilyev, T. L. Merrill, and M. R. Bowlby, "Development of a novel automated ion channel recording method using "inside-out" whole-cell membranes," *SLAS Discovery*, vol. 10, no. 8, pp. 806–813, 2005.
- [14] A. Brüggemann, C. Farre, C. Haarmann, A. Haythornthwaite, M. Kreir, S. Stoelzle, M. George, and N. Fertig, "Planar patch clamp: advances in electrophysiology," *Potassium Channels: Methods and Protocols*, pp. 165–176, 2009.
- [15] L. A. Annecchino and S. R. Schultz, "Progress in automating patch clamp cellular physiology," *Brain and neuroscience advances*, vol. 2, p. 2398212818776561, 2018.
- [16] Q. Zhao, J. Qiu, Y. Han, Y. Jia, Y. Du, H. Gong, M. Li, R. Li, M. Sun, and X. Zhao, "Robotic patch clamp based on noninvasive 3-d cell morphology measurement for higher success rate," *IEEE Transactions on Instrumentation and Measurement*, vol. 71, pp. 1–12, 2022.
- [17] Q. Zhao, M. Wu, M. Cui, Y. Qin, J. Yu, M. Sun, X. Zhao, and X. Feng, "A novel pneumatic micropipette aspiration method using a balance pressure model," *Review of Scientific Instruments*, vol. 84, no. 12, p. 123703, 12 2013.
- [18] Q. Zhao, Y. Han, Y. Jia, N. Yu, M. Sun, and X. Zhao, "Robotic whole-cell patch clamping based on three dimensional location for adherent cells," in *2020 International Conference on Manipulation, Automation and Robotics at Small Scales (MARSS)*. IEEE, 2020, pp. 1–6.
- [19] S. Yang and K. W. C. Lai, "A predictive model for seal condition in an automated patch clamp system," *Journal of Micro and Bio Robotics*, vol. 18, no. 1, pp. 75–87, 2022.
- [20] A. Molleman, *Patch clamping: an introductory guide to patch clamp electrophysiology*. John Wiley & Sons, 2003.
- [21] B. Guan, H. Zhang, and Z. Li, "Basic principles of cellular electrophysiology and patch clamp techniques," 2013.
- [22] W. Dou, Q. Zhao, M. Malhi, X. Liu, Z. Zhang, L. Wang, S. Masse, K. Nanthakumar, R. Hamilton, J. T. Maynes *et al.*, "Label-free conduction velocity mapping and gap junction assessment of functional ipsc-cardiomyocyte monolayers," *Biosensors and Bioelectronics*, vol. 167, p. 112468, 2020.
- [23] P. Jiang, L. Ren, L. Zhi, X. Hu, and R.-P. Xiao, "Protocol for cell preparation and gene delivery in HEK293T and C2C12 cells," *STAR protocols*, vol. 2, no. 3, p. 100497, 2021.